C.P. No. 1146

MINISTRY OF AVIATION SUPPLY

AERONAUTICAL RESEARCH COUNCIL

CURRENT PAPERS

Progress Report on Observations of Three-Dimensional Flow Patterns obtained during Stall Development on Aerofoils, and on the Problem of Measuring Two-Dimensional Characteristics

By

N. Gregory, V. G. Quincey,

C. L. O'Reilly and D. J. Hall

Aerodynamics Division NPL

LONDON: HER MAJESTY'S STATIONERY OFFICE

1971

PRICE 45p net

C.P. No. 1146*
January 1970

Progress Report on Observations of Three-Dimensional Flow Patterns obtained during Stall Development on Aerofoils, and on the Problem of measuring Two-Dimensional Characteristics

- By -
N. Gregory, V. G. Quincey, C. L. O'Reilly and D. J. Hall

SUMMARY

Surface oil-flow patterns were used at low speeds on both thick and thin aerofoils to show the onset of three-dimensionality in either separation or re-attachment when there is an appreciable extent of the separated flow that accompanies the development of the stall. Observations on a thick aerofoil in compressible flow showed a similar trend in the re-attachment behind a shock-induced separation. A form of boundary-layer control applied at the corners at the ends of the aerofoil was able to prevent separation of the corner flow but not to inhibit the development of three-dimensionality.

In order to be able to measure $C_{L\ max}$ with confidence, further experiments are in preparation which will allow the spanwise load distribution associated with the three-dimensionality to be measured. More extensive suction slots and regions of distributed suction are also proposed for the end walls in an attempt to suppress the three-dimensionality.

List of Contents

1./

* Replaces NPL Aero Report 1309 - A.R.C.31 702

1. Introduction

Aerodynamics Division, N.P.L., is currently engaged in a programme of aerofoil development for use on rotor craft. This is being achieved by a continuing process of designing profile modifications and examining theoretical pressure distributions calculated in sub-critical compressible flow. The actual performance of the more promising profiles is checked by two-dimensional tests in both low-speed ($M < 0{\cdot}16$) and, up to transonic Mach numbers, in high-speed wind tunnels ($0{\cdot}3 < M < 0{\cdot}9$). An increase in $C_{L\ max}$ in order to improve the performance of the blade tip is one of the desirable features being sought and achieved. Improvements are required both at low Mach numbers ($M \approx 0{\cdot}4$) for the retreating sector at high forward speed, and at medium Mach number ($M \approx 0{\cdot}6$) for all azimuth positions in hover. The minimisation of pitching moment and the reduction of wave drag are also important for rotor applications. On a rotor, the incidence, Mach number and local sweep all fluctuate with time, and there is a centrifugal force field acting on the rotor-blade boundary layer. Other experiments are needed, therefore, in order to relate the improvements that are obtained in steady two-dimensional flow conditions to those that obtain in the unsteady environment of a rotor. Preparations are in hand for NPL to make a contribution towards this deeper understanding by making measurements on two-dimensional aerofoils undergoing combined pitching and plunging motions at appropriate Mach numbers.

Until such times as this understanding of the unsteady flow is achieved, the theoretical computer programmes that have been developed for calculating helicopter rotor performance both in hover and at forward speed are based on quasi-steady flow conditions, although the downwash variation over the disk due to the periodic vortex wake created by the rotor in earlier revolutions is taken into account. Steady-flow, two-dimensional, sectional characteristics are stored in the computer as reference data, though modifications such as assuming that C_L remains constant at incidences above the stall are made in order to improve the match between measured and calculated rotor performance. This particular modification is very plausible as in conditions close to separation, the centrifugal force field generates a drift of boundary-layer air along the rotor blade which could act as a form of boundary-layer control and go some way towards maintaining constant lift beyond the stall.

The foregoing remarks place considerable emphasis on the accurate measurement of $C_{L\ max}$ over a wide range of Mach number in two-dimensional flow, and knowledge of it is no less important for aerofoils developed for fixed-wing aircraft. However, Moss and Murdin[1] recently encountered considerable difficulty in measuring the lift variation during the pitching oscillation of an aerofoil at the stall because the flow switched intermittently between two distinct types of cycle: in one case the flow unstalled during part of the cycle, in the other it did not. Further examination revealed that in steady flow conditions it was impossible to obtain a fully two-dimensional stall because rear separation moved rapidly forward at one local spanwise position with consequent loss of lift. The part-span vortices at the edges of this initially stalled region induced an upwash between them and a downwash outboard of them, thus stabilizing a "stall-cell" of span less than the span of the model, and which appeared to extend to the end walls only at higher incidence.

It/

It was therefore decided at NPL to investigate carefully the flow encountered in nominally "two-dimensional" test arrangements as the incidence is increased to that at which $C_{L\ max}$ is reached. The investigation seemed essential in view of our current interest in $C_{L\ max}$ in both steady and oscillatory flow conditions. The experiments carried out so far on NACA 0012 in the 36 in x 14 in transonic tunnel are described in Section 2.1. Those in the 13 ft x 9 ft low-speed wind tunnel on this and on another aerofoil section, which also exhibited at low wind speeds a trailing-edge or combined type of stall, are described in Section 2.2. Experiments in the 13 ft x 9 ft wind tunnel on a 7·4% thick aerofoil which exhibited a thin-aerofoil type stall are described in Section 3.

A general discussion follows in Section 4 on the three-dimensional patterns that were found. There is a need to delay their appearance in steady-flow conditions until an incidence above that at which $C_{L\ max}$ is reached so that the accuracy of measurement of this quantity may not be in doubt. For unsteady (oscillatory) flow tests it is desirable to prevent three-dimensional flows from occurring at all, lest their appearance in post-stall conditions alters the way in which unstalled conditions are regained during the decreasing incidence part of the cycle: the three-dimensionality may even be the prime cause of the lack of repeatability experienced by Moss and Murdin[1]. Plans for further experiments to improve our understanding of the phenomena, and which take further steps aimed at completely eliminating the three-dimensional flow régime, are presented and discussed.

2. Stall Development on Aerofoils having Trailing-Edge or Combined Type Low-Speed Stalls

2.1 Observations in the 36 in x 14 in transonic wind tunnel

With subsonic, slotted, liners in position the working section of the 36 in x 14 in transonic wind tunnel is roughly 0·79 m (31 in) high by 0·36 m (14 in) wide and two-dimensional testing is undertaken with 0·36 m (14 in) span models mounted horizontally between schlieren glasses in the walls of the tunnel. Chords of 0·254 m (10 in) or 0·127 m (5 in) are used, giving Reynolds numbers of $1·7 \times 10^6$ or $0·85 \times 10^6$ respectively at $M = 0·3$, increasing to $3·75 \times 10^6$ or $1·88 \times 10^6$ at $M = 0·85$. The ratios of span/chord for these two sizes of model are 1·4 and 2·8 respectively.

Oil-flow patterns obtained on the larger chord model of NACA 0012 at a Mach number of 0·3 are shown in Fig. 1. The patterns were formed by the flow of discrete blobs of oil, which for tests below the stall were applied to the surface in a spanwise row near the leading edge, or for tests at incidences beyond the stall, were applied near the trailing edge. In this Fig., and in all planform views of oil flows except for Figs. 3 and 5, the pictures have been cropped at the edges of the model. The ends of long oil-flow streaks indicate the approximate position of flow separation, and this is confirmed by the accumulations of oil that can be seen, showing that separation was the reason for the termination of the flow rather than the running out or drying out of the oil. At 11° incidence ($C_L = 1·09$), turbulent boundary-layer separation occurs ahead of the trailing edge (at $x/c = 0·84$ at mid-span), and rapid growth of the end-wall boundary layers is indicated by the divergence of the end oil-flow streaks from the adjacent walls. At 12·5°, which corresponds to maximum measured C_L of 1·15, Fig. 2, separation is further forward at mid-span (0·75c), but

back/

back at the trailing edge just outside the tunnel-wall boundary layer. At one end, the corner flow is completely separated. Above 12·5°, the aerofoil is completely stalled intermittently and no meaningful oil pattern can be obtained until an incidence setting of 14° is reached and the aerofoil is stalled all the time. The oil-flow pattern then shows a curved separation line located at 0·04 c at mid-span, but bending back as it nears the tunnel-wall boundary layer, just outboard of which lies a singular spiral separation point, Fig. 1f. In these conditions, the flow right in the corner is flowing in a rearwards direction and away from the corner, as can be seen from Fig. 3.

Also shown in Fig. 3 are oil-flow patterns obtained at two higher Mach numbers at incidences close to the stall (Fig. 2). At these Mach numbers the stall is due to shock-induced separation and the separation fronts are much more nearly two-dimensional than those at a Mach number of 0·3, though again both shock and separation terminate at the outer edge of the wall boundary layer. The flow was indicated by oil distributed either uniformly over the surface or locally in blobs, and at both $M = 0{\cdot}65$ and $M = 0{\cdot}825$, flow re-attachment occurred along a curved front, the separation bubble being much longer at mid-span than it was nearer to the tunnel walls. Thus as in the stalled flow case at $M = 0{\cdot}3$, the distribution of trailing vorticity is such as to induce an upwash in the centre of the span, thus maintaining stalled flow, and a downwash close to the tunnel walls, thus maintaining separation-free flow. Oil-flow patterns on the end wall for the three pre-stall cases of Fig. 3 are given in Fig. 4. They clearly show the presence of the well-known horse-shoe vortex lying in the end-wall boundary layer, and wrapped round the obstacle (i.e. the aerofoil), which protrudes through the layer. The photographs vividly demonstrate that the flow in the corner between the model and the end wall is not the undistorted tunnel-wall boundary layer approaching the model. The great width on the tunnel wall towards the rear of the aerofoil of the region between the two branches of the three-dimensional separation line when the aerofoil is at high angles of incidence should also be noted.

The region of trailing vorticity when shock-induced separation occurs lies close to the outer edge of the boundary layer. This is to be expected since the shock disappears at the edge of the layer, as the velocities in the layer rapidly become wholly sub-critical. In the low-speed ($M = 0{\cdot}3$) stalled-flow case the trailing vorticity also lies close to the outer edge of the wall boundary layer (which in undisturbed conditions is about (25 mm) 1·0 in thick), but not in Fig. 5, which shows the development of the stall at a Mach number of 0·3 on the 0·127 m (5 in) chord model. Here, the rates of tunnel-wall boundary-layer thickness to aerofoil chord is much larger, and adverse pressure gradients due to the aerofoil are more intense, the corner-flow separates at a lower angle of incidence and the reverse-flow region on the aerofoil penetrates further towards the centre of the tunnel. The aerofoil finally stalls at about 1° lower incidence than is the case at double the Reynolds number. The trailing vorticity, which has opposite sense to that trailed from the corner separation, is then well outside the boundary layer, and is strong enough to induce sufficient downwash between itself and the tunnel wall to prevent corner separation. At 12° mid-span turbulent separation is further aft than at 14° at double the Reynolds number, and in consequence the separation front is more highly curved. It should also be noted that the port tunnel-wall boundary layer is slightly thicker than that of the starboard one and exhibits separation at a slightly reduced incidence; in Figs. 1 and 5 this shows up at the right-hand end of the model, as these photographs were taken looking upstream with the aid of a 45° inclined mirror held above the model.

2.2 Observations in the 13 ft x 9 ft low-speed wind tunnel

The possibility of separation of the corner flow in tests at a Mach number of 0·16 in the 13 ft x 9 ft wind tunnel had been foreseen, and provision for boundary-layer control to prevent it had been made.[2] The provision took the form of a fixed suction slot in the end walls of the wind tunnel just ahead of the leading edge of the aerofoil. Near stalling incidence, the slot extended for a distance roughly equal to the aerofoil thickness on either side of the chord line. Into this slot was sucked air at a rate which ensured that about one half the undisturbed boundary layer was removed over the span of the slot. This implied removing boundary-layer flow from the region between the surface and the point where the velocity was 0·95 of the free-stream value. In addition to this, 0·304 m (1 ft) of span at each end of the 2·74 m (9 ft) span model was perforated with 6 rows of closely pitched holes distributed between the leading edge and the 0·03 chord position on the upper surface. Distributed suction here, in combination with slot suction, ensured that the stall was no more likely to start at the ends of the span than at any other position.

Detailed oil-flow observations in the 13 ft x 9 ft wind tunnel were carried out on NPL 9619, as this was the section under test at the time the desirability of exploring flow conditions in the neighbourhood of the stall first became apparent. NPL 9619 was developed from NACA 0012 by the introduction of a droop-nosed extension. The resulting aerofoil had a chord of 0·83 m (32·8 in) with a span/chord ratio of 3·29 and was 11·0% thick. The camber line was closely similar to the NACA 230 camber line. The variations of lift coefficient and position of turbulent-boundary-layer separation with incidence at a Reynolds number of $3·14 \times 10^6$ ($M = 0·16$) are shown in Fig. 6 for a variety of transition-free test conditions. The corresponding curve for the 0·76 m (30 in) chord model of NACA 0012 tested at the same wind speed with similar boundary-layer control arrangements has been added for comparison: Ref. 2 indicated that there was some scatter in the recorded values of $C_{L\ max}$ for this section, which are some 0·02 to 0·09 less than the value of $C_{L\ max}$ obtained on the cambered variant. Later, a few check oil-flow observations were taken on the NACA 0012 section, and showed that the stall development followed the pattern obtained on NPL 9619, though corresponding stages were of course reached at slightly different incidences and lift coefficients.

Pictures of oil-flow patterns on the surface of the NPL 9619 model and on the end wall, which were taken to indicate the development of the stall, are shown in Figs. 7-12. For these photographs, with one exception, liberal blobs of oil were applied in a regular pattern over the surface of the model. In order to obtain suitable contrast between the oil-flow patterns and the natural finish of the bare aluminium models and to avoid troublesome lighting reflections, saturn-yellow "Dayglo" powder was added to the normal oil mixture used in the low-speed tunnel tests and the pattern was illuminated solely with a 40 W. ultra-violet fluorescent lamp. This caused the pigment to fluoresce with a light green light, and this was photographed using a dark green filter. The boundaries of the model were defined by means of strips of paper coated with the saturn yellow placed partly behind the leading and trailing edges of the aerofoil.

It/

It must also be appreciated that the model stood vertically in the wind tunnel so that in regions of weak shear, gravity forces gave a downward bias to the oil-flow. A further reservation needs to be made. Although the photographs are loosely described as showing stall-development, they were obtained by applying the oil, setting the incidence and then raising the wind speed from zero to the test value. Now the Reynolds number of these tests was around 3×10^6, which was higher than the values of $0{\cdot}85 \times 10^6$ and $1{\cdot}7 \times 10^6$ obtained in the runs at low Mach number in the transonic tunnel (Figs. 5 and 1) and the stall occurred at a higher incidence because of favourable scale effects. Even in the steady-flow conditions which are reached following slowly-made changes, therefore, the stall is a function of incidence and Reynolds number as well as the direction in which these parameters are changed, since there may be a difference in the corresponding movements of separation and re-attachment fronts. The stall thus develops either as a result of increasing incidence at constant Reynolds number, or if the incidence lies in a high but narrow band, by reducing Reynolds number at constant incidence. It is not proven that the patterns that develop are identical, and indeed suction peaks behave differently in the two cases; but if we assume that the patterns are identical, then the patterns of Figs. 7-12, obtained at fixed incidence by increasing Reynolds number from zero, should be regarded as equivalent to those obtained at fixed Reynolds number by reducing the incidence to the stated value from a higher one, and so indicate the collapse of the stall. Therefore, where there is a hysteresis loop in the lift incidence relations the patterns relate to the lower return branch and do not necessarily represent the situation which might obtain when the stall is approached at constant Reynolds number (or wind speed) by increase in incidence. Such patterns cannot readily be obtained since, if oil is applied to the surface when the wind speed is zero, a conflicting and unwanted pattern is obtained during the process of raising the wind speed to the required value. For this reason, as commented on later, one aerofoil model is being modified for an oil injection technique which will allow the oil to be applied when the required conditions have been established. This also avoids a further source of confusion, that separated flow present during flow acceleration is to some extent suppressed and modified by the acceleration itself. Oil-flow patterns close to the stall far more frequently show signs of two distinct flow régimes than the samples selected for this paper might lead the reader to imagine.

It should be noted that the individual observations of lift coefficient and incidence for NPL 9619 shown in Fig. 6 were measured during oil-flow observations, and no great difference was noticed when lift was measured after increasing incidence at constant wind speed. NACA 0012, however, appeared to show more hysteresis[2], and lack of repeatability was encountered for other reasons: the curve for NACA 0012 shown in Fig. 6 was obtained by increasing incidence at constant wind speed, 55 m/s (180 ft/s).

The general pattern of Fig. 7 resembles that of Fig. 5. As the turbulent separation front moves forwards, strict two-dimensionality is upset by the appearance of a large region of separated flow in the corner. The change in the flow over the end wall is shown in Figs. 8a and b. At 16° (Fig. 7), just below the incidence at which $C_{L\ max}$ is reached, it will be noticed that the reverse flow region downstream of turbulent separation contains spanwise components, the flow converging towards mid-span. Finally, at 18° the mushroom-shaped stall cell is established, outside which the upwash is sufficient to eliminate the top corner separation. At 19° the pattern has shifted downwards: the bottom corner separation has disappeared and been replaced by separation in the top corner. The 20° pattern is novel. Two complete stall cells are present with attached flow along the centre line and in the corners. Unfortunately the lift coefficient of 1·13 shown in Fig. 6 was obtained at

a different time, without an oil-flow picture, and it is not known whether this value is appropriate to the twin-cell pattern. On another occasion, the upper suction slot and perforations were left unsealed. Although there was no net suction flow, this permitted inflow to both slot and perforations in the region of higher external static pressure, with balancing outflow in the region of peak suction. This of course precipitated flow separation in the top corner and resulted in the pattern of Fig. 9.

The use of discrete blobs of oil does not show up clearly any weak convergence of the flow toward a three-dimensional separation line. Fig. 8c uses a distributed oil-film to show that in the absence of any flow into the floor suction slot (which was sealed), such a line is present in the flows of Figs. 8a, b, as in the transonic tunnel tests of Fig. 4.

Stall development was also examined with a standard flow rate into the suction slot, and with flow into the rows of perforations. The perforations were either 0·18 c or 0·36 c in extent. Fig. 10 shows the oil-flow patterns obtained with the shorter length of perforations (C_Q = 0·0018). Although corner separation is completely eliminated, the formation of a three-dimensional stall cell has not been inhibited. The maximum lift coefficient was recorded at 17° with turbulent separation at 0·8 c mid-span and the oil-flow pattern already shows the beginnings of a mushroom-shaped separation front. At 20° incidence, the separation front is well forward and nearly parallel to the leading edge, but strong spanwise flow components remain over much of the span, both ahead of and behind separation. Similar results were obtained with suction into the 0·36 c length of perforations except that the slightly reduced inflow rate (C_Q = 0·0013) then applied was insufficient to prevent separation of the flow in the top corner at 17° and 17·5°. This however could be stopped by a little blowing from the blowing slot installed in the tunnel wall immediately downstream of the suction slot. The only other noteworthy difference was at 20°, where there was a slight indentation in the separation line at mid-span. Separation here was perhaps 0·1 c further aft than at mid- semi-span, giving the impression of an incipient breakdown into the twin-cell pattern of Fig. 7.

An attempt was made to simulate the span/chord ratio of the 36 in × 14 in transonic tunnel tests by fitting large fins in a part-span position, symmetrically disposed on either side of mid-span. The span/chord ratio was 1·28 or 1·4 depending on whether or not the aerofoil had an extended nose. The fins used (2·0 c chord × 1·2 c span) proved insufficient to entirely isolate the aerofoil between them from induced flow effects arising from a change of flow régime over the end portions of the aerofoil, but Fig. 11 shows the oil-flow patterns obtained during stall development. It is very interesting that the maximum recorded C_L was raised by more than 0·1 to a value of 1·7 without any use of boundary-layer control (Fig. 6). This maximum lift was recorded at 18·5° geometric incidence. The oil-flow patterns at this incidence and at 18° show an intermittent flicking between the unstalled-type pattern of 17° and the fully-developed stall cell of 19° incidence setting. The staggered positions of the singular separation points within the confines of the part-span fins is interesting. They are not located by any geometrical features of the model and their position could be self-induced by the vortices which spring from them (somewhat analogous to the stable arrangement of a Kármán vortex street). Alternatively it might merely reflect an asymmetry in the induced flow resulting from some difference in the flows over the top and bottom outer portions of span. It is not clear which is the case.

In/

In an endeavour to simulate the transonic wind-tunnel arrangements more closely, narrow transverse strips of gauze were fitted at the leading edges of the fins to thicken the fin boundary layers to the same thickness (measured in terms of the wing chord) as the wall boundary layers in the transonic tunnel. Measurements were taken at 17° (near $C_{L\ max}$) and in stalled flow at 20°, Fig. 12. C_L was appreciably less at 17° (Fig. 6) although the flow appeared not to be stalled, but was not significantly reduced at 20°. In both cases, the two-dimensionality of the flow was spoilt (Fig. 12) by massive corner separations which continued to dominate the flow even in the stalled case of 20°, so that in this condition there was no sign of the mushroom-shaped stall cell that occurred in the transonic wind tunnel (Fig. 1f)

On NACA 0012, check observations showed that the general development of stalled flow with boundary-layer control applied followed closely the development of Fig. 10. The only noticeable difference was that the well-developed stall cell was found at either the top or the bottom of the span (as at 19° in Fig. 7, but without a corner separation), rather than in a symmetrical position, as at 17·5° in Fig. 10. In asymmetric conditions, the mid-span flow is not two-dimensional nor does it lie along the line of pressure holes. With fins present, limiting the span/chord ratio to 1·4, the stalled-flow pattern usually found can best be described as half a stall-cell, sometimes with some rearward movement of separation at that end of the pattern which would normally be the plane of symmetry of a complete cell. Fig. 13 shows an example of a lower half-cell, but some difficulty was experienced in obtaining pictures showing a single flow régime as the régime intermittently switched from being a bottom half to being a top half of a stall cell.

The discovery of a double stall-cell pattern, Fig. 7 (20°), raises the question of what determines the span of a mushroom-shaped stall cell when it first appears. Is it related to the chord or the span of an aerofoil? Can a stall cell of limited span exist in the middle of a long two-dimensional aerofoil without reference to the conditions at the tunnel walls, or is the spread of a stall cell (assuming it starts in mid-stream) stopped only by some image or constraint effect in the end walls? A search for limited-span cells was therefore undertaken with an available NACA 0012 aerofoil of span/chord ratio of 6 mounted between larger end plates (2·25 c span × 3·75 c chord) in the 13 ft × 9 ft wind tunnel.

The development of the stall on this model is shown in Fig. 14. The aerofoil had a chord of only 0·203 m (8 in) and therefore at the same wind speed as before, the Reynolds number was only $0{\cdot}76 \times 10^6$. At this Reynolds number a laminar separation bubble is seen to remain passive at the leading edge throughout, and the stall develops between 13·3° and 13·75° geometric incidence by the forward movement of rear turbulent separation. At 13·4° the pattern reverted, in the course of the run, from a single stall cell with mid-span separation at 0·5 c to the more nearly two-dimensional conditions with separation at perhaps 0·75 c. At 13·5°, a repeat run yielded an "unstalled" pattern indistinguishable from that shown for 13·3°. The pattern at 13·75° started as that at 13·5°, i.e. as a full-span stall cell, but after half a minute's steady running it changed to that shown where the oil at mid-span and mid-chord is continually flicking to and fro, as if the pattern is about to break down to two stall cells.

To date, therefore, a limited-span stall cell appears not to be a likely flow form on this long-span model, though it must be admitted that the patterns were once again obtained with the incidence pre-set and developed as the wind speed increased to the test value. This model was however intended

to/

to utilise a novel form of oil injection, which consisted of a tube embedded in the model carrying the pigmented oil and a number of valves connected this tube to two rows of surface holes. Raising the oil pressure would allow oil to be released onto the surface after the correct working conditions had been established and the pattern formed should be free of transient effects generated during the acceleration of the airstream to test speed. Unfortunately the valves have required further development in order to obtain satisfactory performance. It remains possible, however, that a limited-span stall cell may only appear when incidence is increased at constant wind speed, and so a definite conclusion will not be reached until the model has been tested in this mode. It also now appears that this may be the only value of the plumbing system on this model, for Erlich[3] finds on another aerofoil that hysteresis effects at the stall are confined to the limited Reynolds number range in which stall is precipitated by the "bursting" or failure to re-attach of a laminar separation bubble. It seems likely that the test Reynolds number of $0{\cdot}76 \times 10^6$ on this model lies below this range, and in any case there is some doubt as to whether the stall of NACA 0012 is of this type.[2]

3. Stall Development on an Aerofoil exhibiting Thin-Aerofoil Stall

NPL 9621 is a symmetrical section, 7·38% thick, having a large value of the nose radius, 0·0100 c, compared with a value 0·0060 c for a NACA four-digit aerofoil of the same thickness/chord ratio. Despite the unusually large nose radius, the aerofoil exhibits the thin-aerofoil stall expected of an aerofoil of this thickness (at 0·0125 c) and just lies within Gault's region of correlation[4] for stalls of this type. Variation of lift coefficient with incidence for a variety of test conditions is shown in Fig. 15. It will be noted that there is a large hysteresis around the stall.

Since incidence was set before the tunnel wind speed, the oil-flow patterns shown in Fig. 16 relate to the return branch of the lift loop. At 8° and above, the flow separates at the leading edge and re-attaches further back along the aerofoil along fronts whose positions are traced in Fig. 17, although the topology of the situation is not entirely clear. As long as some re-attachment occurs, a twin-cell pattern occurs, the flow along the centre line of the tunnel remaining attached downstream of a short bubble. At 13°, however, the pattern is difficult to interpret.

As before, it must be emphasized that Fig. 16 illustrates effectively a sequence showing the collapse of the stall as the incidence decreases from the high values to the low ones. Less precise indications given by tufts distributed over the surface showed that as incidence increased, appreciable regions of separated flow developed over the top half of the model. Separation on the lower half remained confined to the region of the short bubble presumed to occur at the leading edge since the rearward spread occurred only at about 2° higher incidence than that on the top half of the aerofoil. When incidence was decreased, however, as in Fig. 16, both regions of separation shrank simultaneously. Although with incidence increasing the top half of the model always stalled first, it was found possible to reverse the sequence by attaching lumps of plasticine to the leading edge on the lower half of the wing and forcing separation there. Again, a 2° lag in incidence occurred before the flow over the top half of the aerofoil separated. As before, both separated regions shrank in size together as incidence was decreased.

On this aerofoil, corner separation appeared not to be a great problem (Fig. 16) and so there seemed no reason to apply boundary-layer control at the ends of the span. Nevertheless, when it was applied an increase in $C_{L\ max}$ was realised, Fig. 15, for reasons which are not obvious.

The/

The aerofoil was also tested with fins fitted 1·4 chords apart. The pattern (Fig. 18) remains the same as that found on the same region of the full-span aerofoil. When the flow fails to re-attach, an S-shaped surface-flow pattern is clearly marked. Similar patterns are also found (Fig. 19) when the boundary layers on the facing surfaces of the fins were thickened up to simulate those in the transonic tunnel. Corner separations (especially at the lower end of the model) are again evident, but do not dominate the stall as they did in the case of the rear-stalling aerofoils.

4. General Discussion and Proposals for Future Work

The observations described in detail in the previous Sections show that at high angles of incidence of an aerofoil having attached flow over its nose, the flow in the corner between the aerofoil and the tunnel wall is inclined to separate before the flow over the centre of the model, thus upsetting two-dimensional flow conditions. This corner separation was suppressed (on an unflapped aerofoil) by suction through short lengths of the slot at the front edge of the corner. The slots ran normal to the free-stream along each tunnel wall, and extended on each side of the aerofoil for a distance of the order of the thickness of the aerofoil. Along the upper surface of the aerofoil there were 6 rows of closely pitched perforations extending for a distance of the order of the undisturbed boundary-layer thickness on the end wall. For the present unflapped aerofoils, this arrangement seems to be an alternative to suction into a slot running along the length of the corner used by Foster and Lawford [5], but an exact comparison is not possible because no attempt has been made in the present investigation, so far, to measure the uniformity of lift loading that has resulted. As the chordwise extent of separation over the rear of an aerofoil grows with incidence, it has been found that the separation becomes three-dimensional in character and this development has not been affected by suppression of the corner flow separation.

The three-dimensional development occurs when the chordwise extent of separated flow exceeds about 0·2 chord and shows up as curvature of the turbulent boundary-layer separation front, with pronounced spanwise flow components In the case of flow separation occurring at the nose of the aerofoil, or immediately downstream of a shock wave, the separation front remains straight and the subsequent re-attachment front is curved.

The spanwise variations seem to be affected by the aerofoil profile and by the ratio of span to chord. For a given profile in two-dimensional flow, relations connecting lift coefficient with incidence and positions of flow separation (and re-attachment if this occurs), which are further modified by induced camber effects, ought to determine a spanwise variation in separation given an initial variation in incidence and camber. This variation is caused by the induced flow due to the trailing vorticity associated with the resulting spanwise distribution of lift. The stall cell thus formed has a more extensive separation mid-stream, and less so at its extremities, and this is consistent with mid-stream upwash between two trailing vortices and downwash outside them. Two cells are present side by side when separation occurs at the aerofoil leading edge, and have occasionally been found when separation occurs further aft. Efforts to determine whether there is a preferred ratio of cell span/wing chord other than that given by a span slightly less than the wing span have not yet clarified the situation. Indeed, until an isolated cell of really limited span is found it is not possible to conclude that the tunnel wall or tunnel-wall boundary layer do not play an essential part in the process. Whether or not corner separation exists, there are marked spanwise flow components. Yet a strong stall cell can itself induce sufficient downwash to suppress corner separation, and the development of the stall cell seems not to be influenced by application of the present form of boundary-layer control.

Further/

Further experiments are therefore desirable in which not only should measurements of spanwise lift loading be made in the presence of a stall cell, but further efforts made to suppress the three-dimensional development. This accomplishment would have important consequences for the improvement of existing wind tunnels and for the detailed design of new facilities for measuring two-dimensional aerofoil characteristics, whether at high Mach number or low.

Some work on the reduction of end wall boundary-layer thickness in a high speed tunnel, carried out as a preliminary to further investigations of three-dimensional effects at high speeds, has recently been published by Hall[6].

References/

References

No.	Author(s)	Title, etc.
1	G. F. Moss and P. M. Murdin	Two-dimensional low-speed tunnel tests on the NACA 0012 section including measurements made during pitching oscillations at the stall. RAE Tech Report TR 68104. May, 1968. A.R.C.30 682. To be A.R.C. C.P.1145.
2	N. Gregory and C. L. O'Reilly	Low-speed aerodynamic characteristics of NACA 0012 aerofoil section, including the effects of upper surface roughness simulating hoar frost. NPL Aero Report 1308. January, 1970. A.R.C.31 719.
3	E. Erlich	Contribution to Euromech Conference, Stockholm. June, 1969. Exemples des recherches sur les profiles dans la soufflerie S10 du CEAT à Toulouse. ONERA. Tiré à part TP No.766. 1969.
4	D. E. Gault	A correlation of low-speed airfoil section stalling characteristics with Reynolds number and airfoil geometry. NACA TN 3963. March, 1957.
5	D. N. Foster and J. A. Lawford	Experimental attempts to obtain uniform loading over two-dimensional high-lift wings. RAE Tech Report TR 68283. December, 1968. A.R.C.31 098.
6	D. J. Hall and V. G. Quincey	Some experiments on a wind tunnel wall boundary-layer bleed at high subsonic speeds. NPL Aero Note 1093. A.R.C.32 357. September, 1970.

BMG

FIG.1 (a–c)

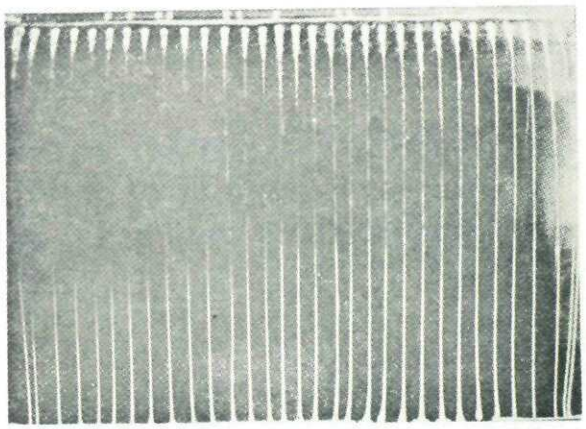

Flow direction

(a) $M = 0.3$ $\alpha = 8^0$ $C_L = 0.82$

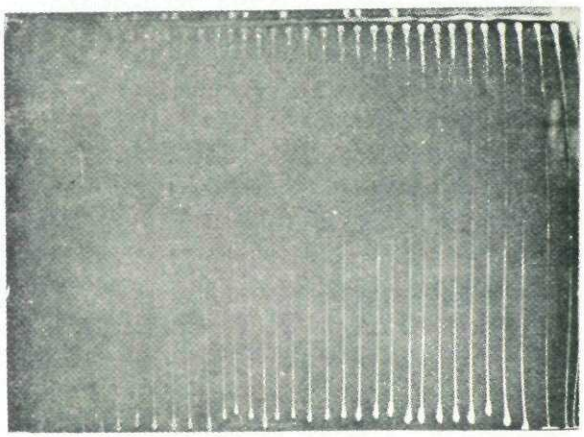

(b) $M = 0.3$ $\alpha = 9^0$ $C_L = 0.93$

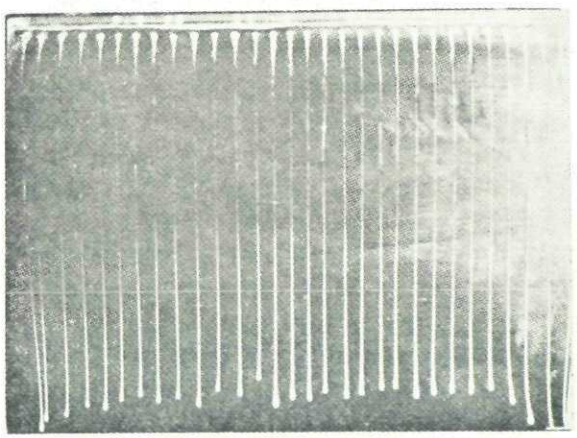

(c) $M = 0.3$ $\alpha = 10^0$ $C_L = 1.02$

Oil-flow patterns on 0·254 m (10 in.) chord model of NACA 0012 in 36 in. x 14 in. transonic tunnel at $M = 0.3$. Span / chord = 1·4. $R_c = 1.7 \times 10^6$

FIG. 1 (d-f)

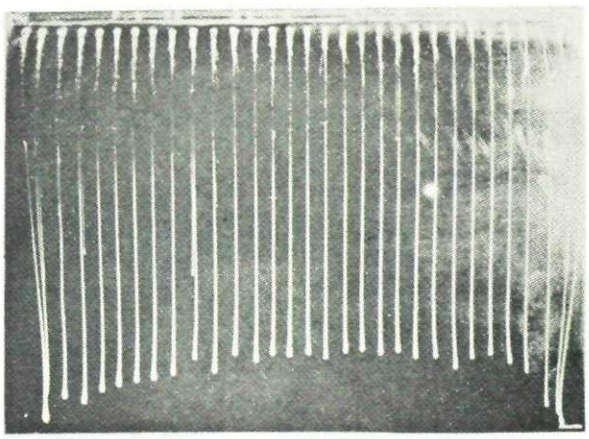

Flow direction

(d) $M = 0.3$ $\alpha = 11^{\circ}$ $C_L = 1.09$

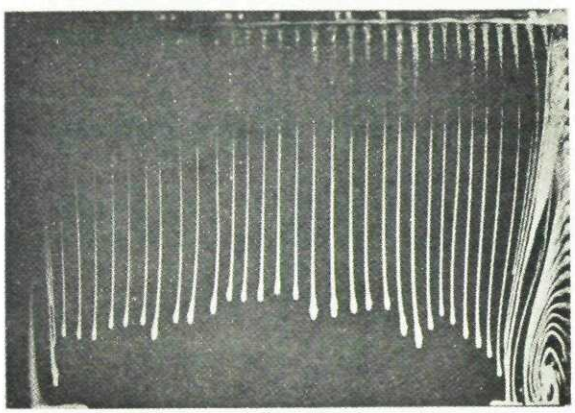

(e) $M = 0.3$ $\alpha = 12.5^{\circ}$ $C_L = 1.15$

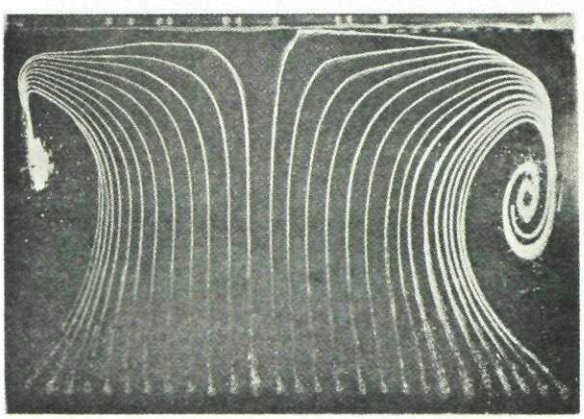

(f) $M = 0.3$ $\alpha = 14^{\circ}$

Oil-flow patterns on 0·254 m (10 in.) chord model of NACA 0012 in 36 in. x 14 in. transonic tunnel at $M = 0.3$. Span/chord = 1·4. $R_c = 1.7 \times 10^6$

FIG. 2

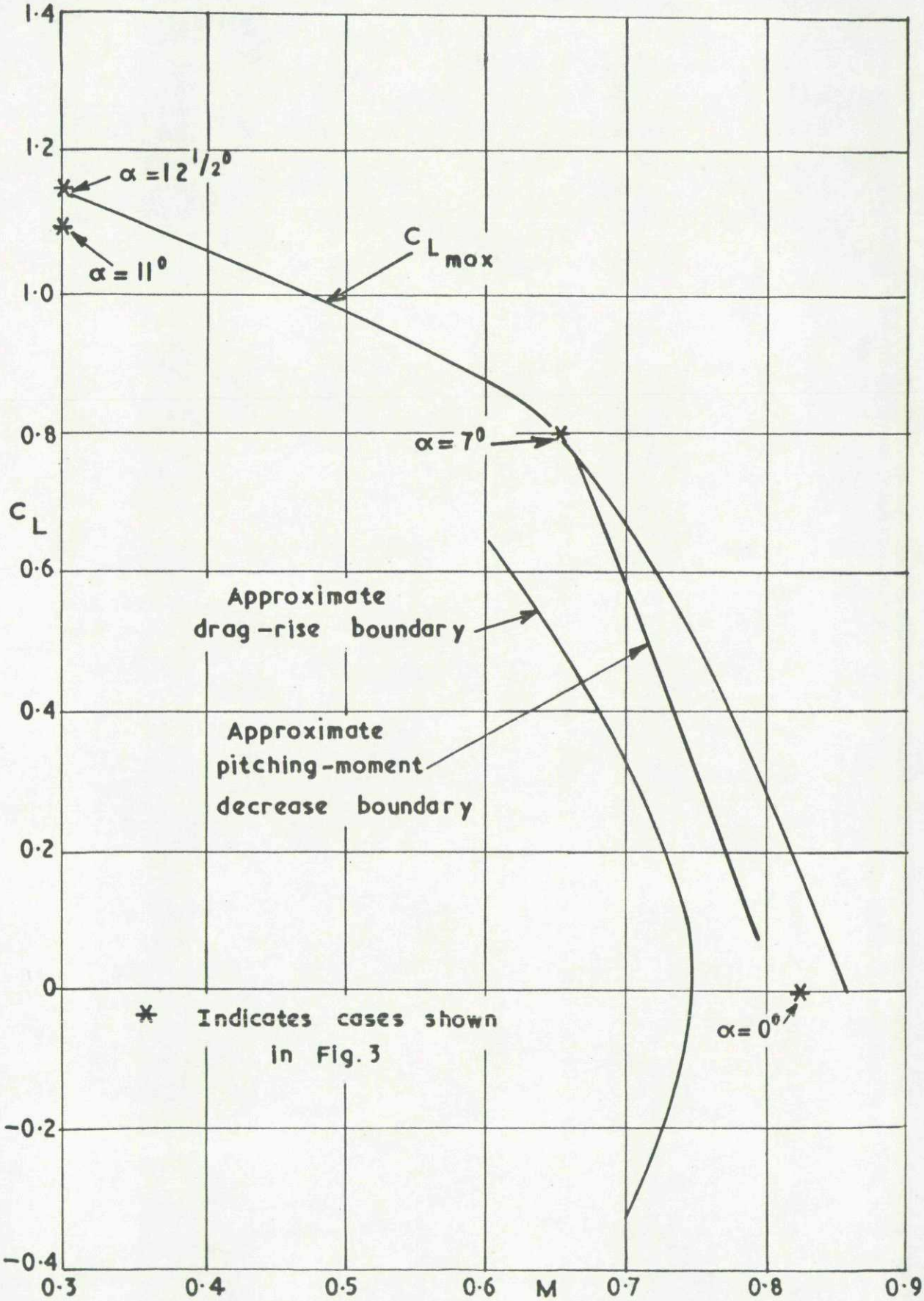

Limiting boundaries for NACA 0012 measured in the 36 in. x 14 in. transonic tunnel

FIG. 3

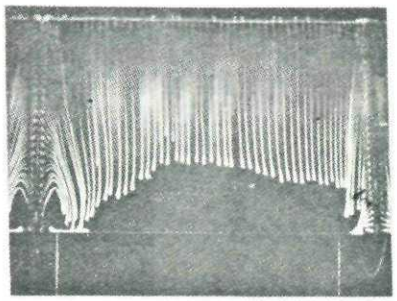

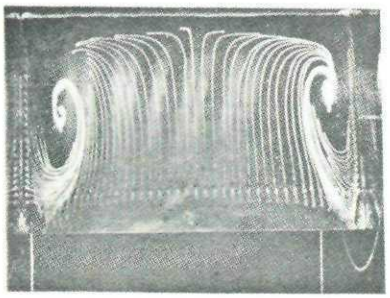

Flow direction

$M = 0 \cdot 3 \quad \alpha = 12 \cdot 5^0 - 14^0 \quad C_L = 1 \cdot 15$ at $12 \cdot 5^0$

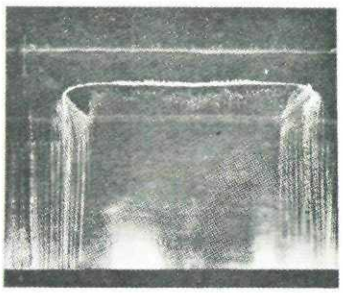

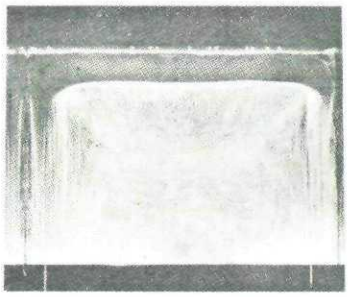

$M = 0 \cdot 65 \quad \alpha = 7^0 \quad C_L = 0 \cdot 78$

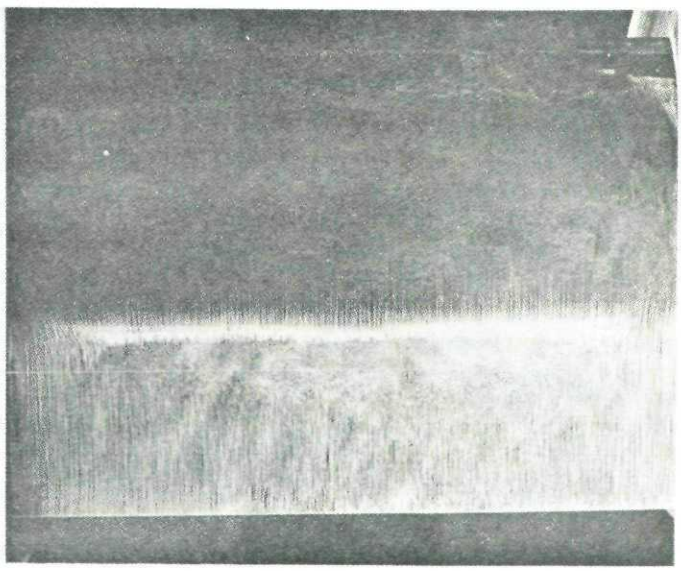

$M = 0 \cdot 825 \quad \alpha = 0^0 \quad C_L \approx 0$

Oil-flow patterns on 0·254 m (10 in.) chord model of NACA 0012 in 36 in. x 14 in. transonic tunnel at three conditions close to $C_{L\,max}$

FIG.4

Flow direction →

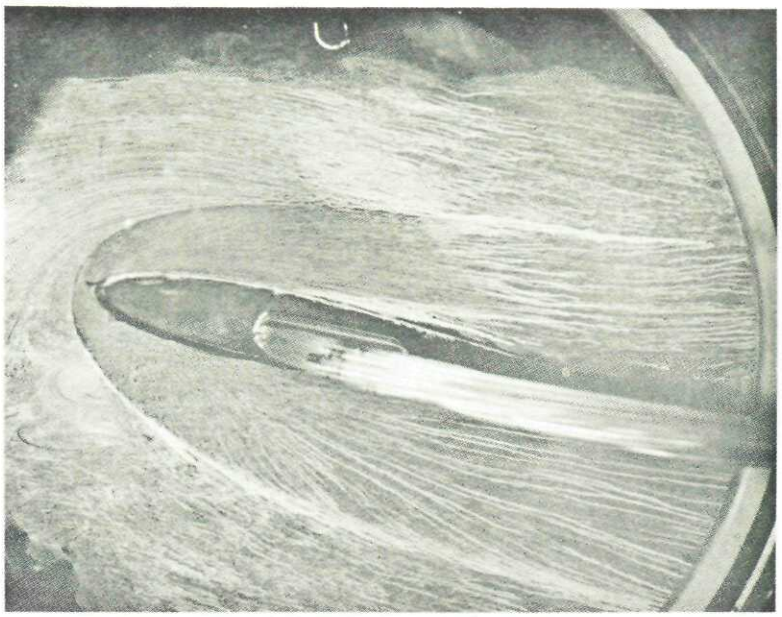

M = 0·3
α = 12·5°

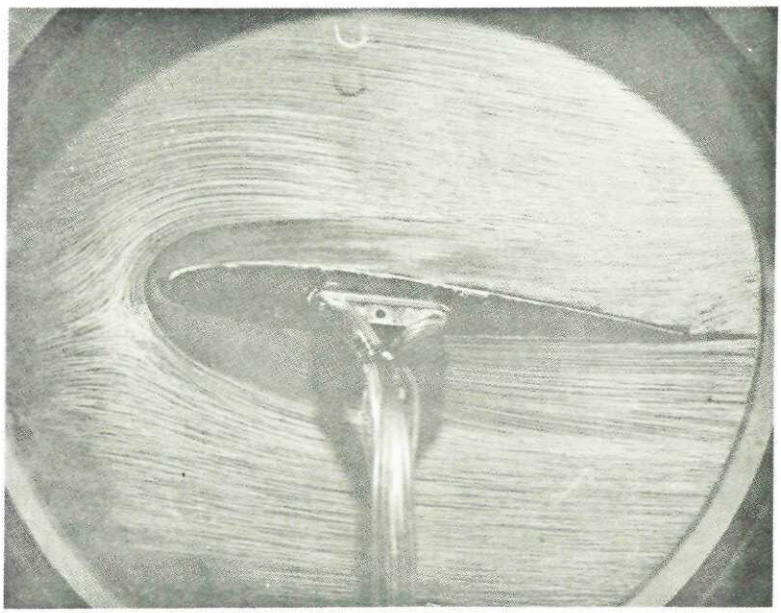

M = 0·65
α = 7°

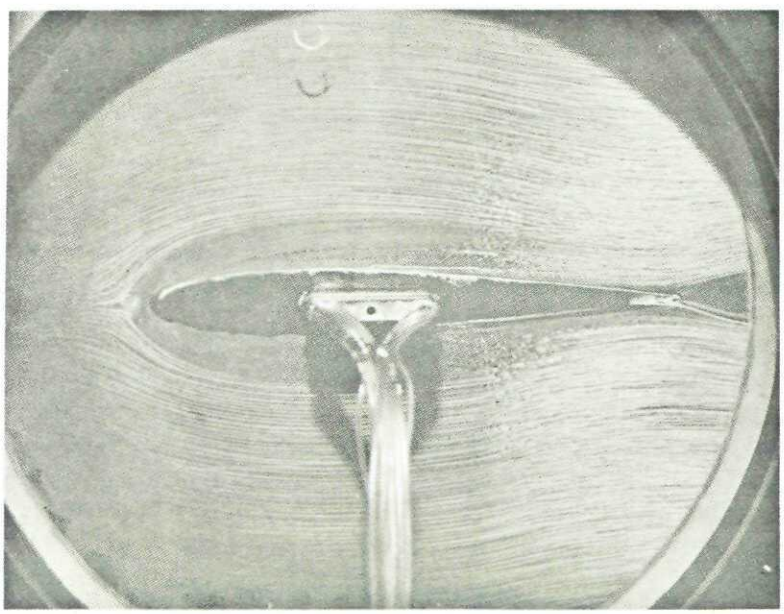

M = 0·825
α = 0°

End-wall oil-flow patterns for the three pre-stall cases of Fig. 3

FIG.5

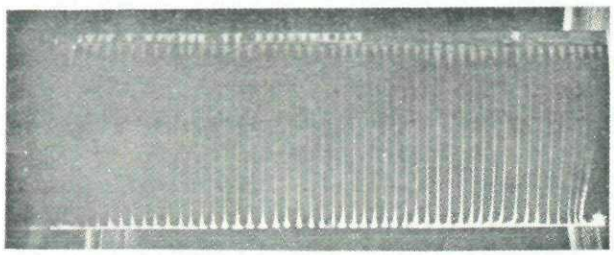

(a) 7°

Flow direction

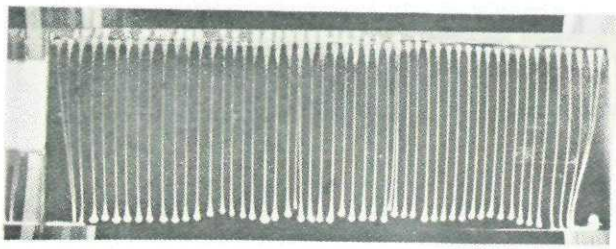

(b) 8°

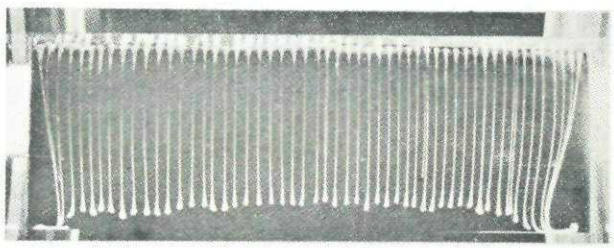

(c) 9°

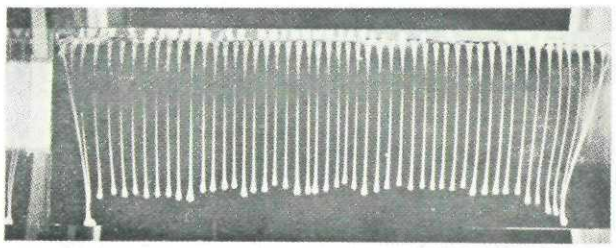

(d) 10°

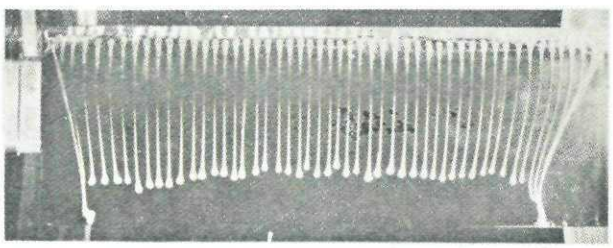

(e) 11°

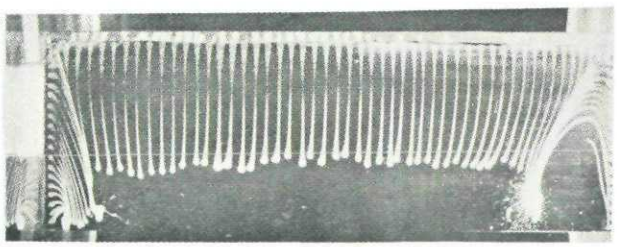

(f) 11·5°

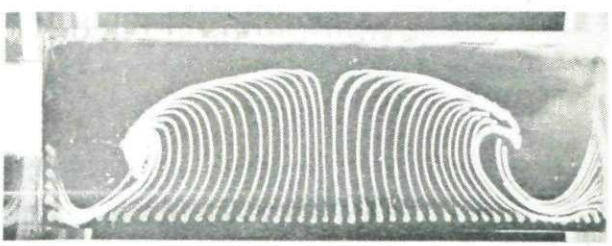

(g) 12°

Oil-flow patterns on 0·127m (5 in.) chord model of NACA 0012 in 36 in. x 14 in. transonic tunnel at M=0·3. Span/chord = 2·8. R_c = 0·85 x 10^6

FIG.6

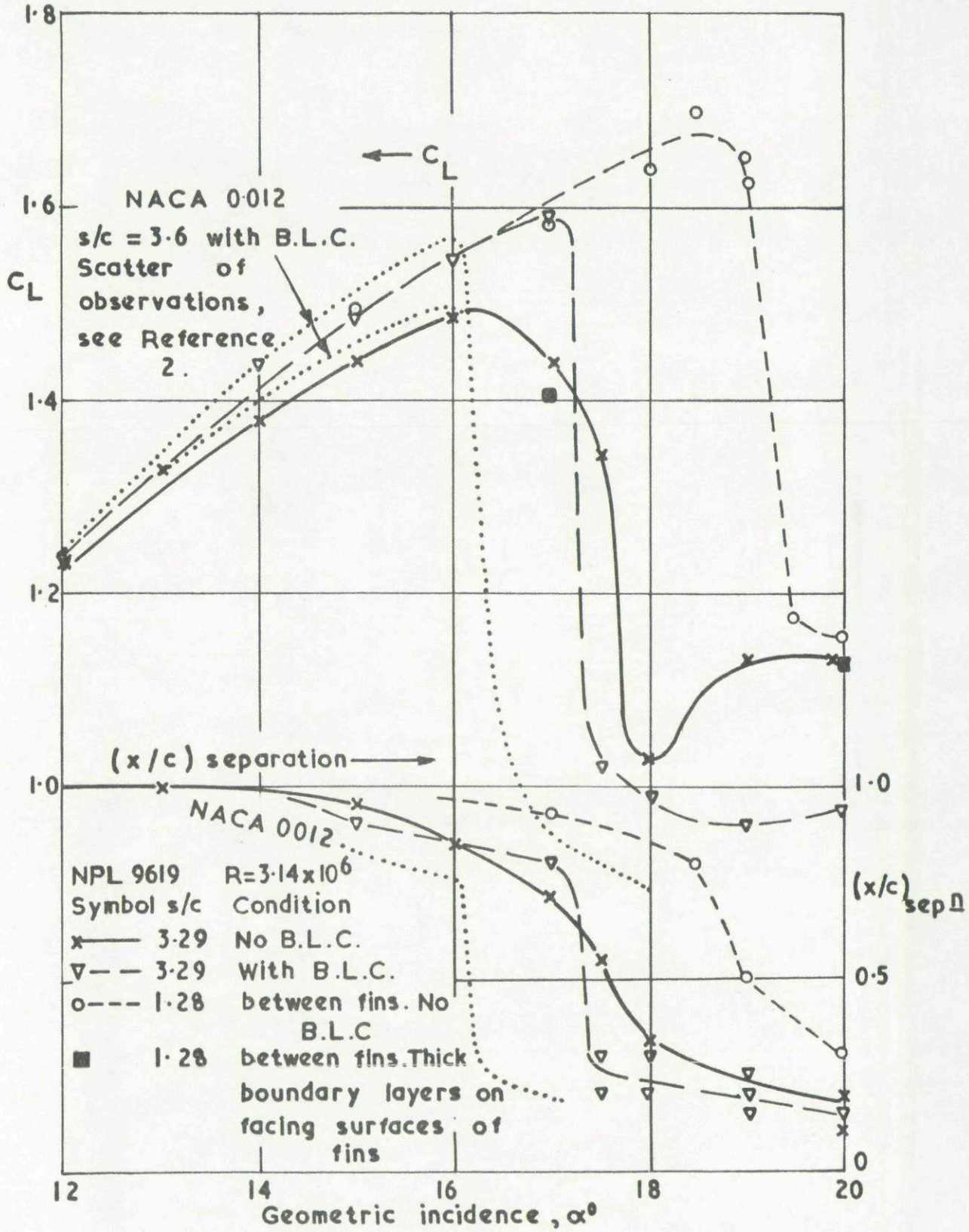

Variation of lift coefficient and turbulent-boundary-layer separation position with incidence for NPL 9619 and NACA 0012 in various test conditions in 13 ft x 9 ft tunnel

FIG. 7

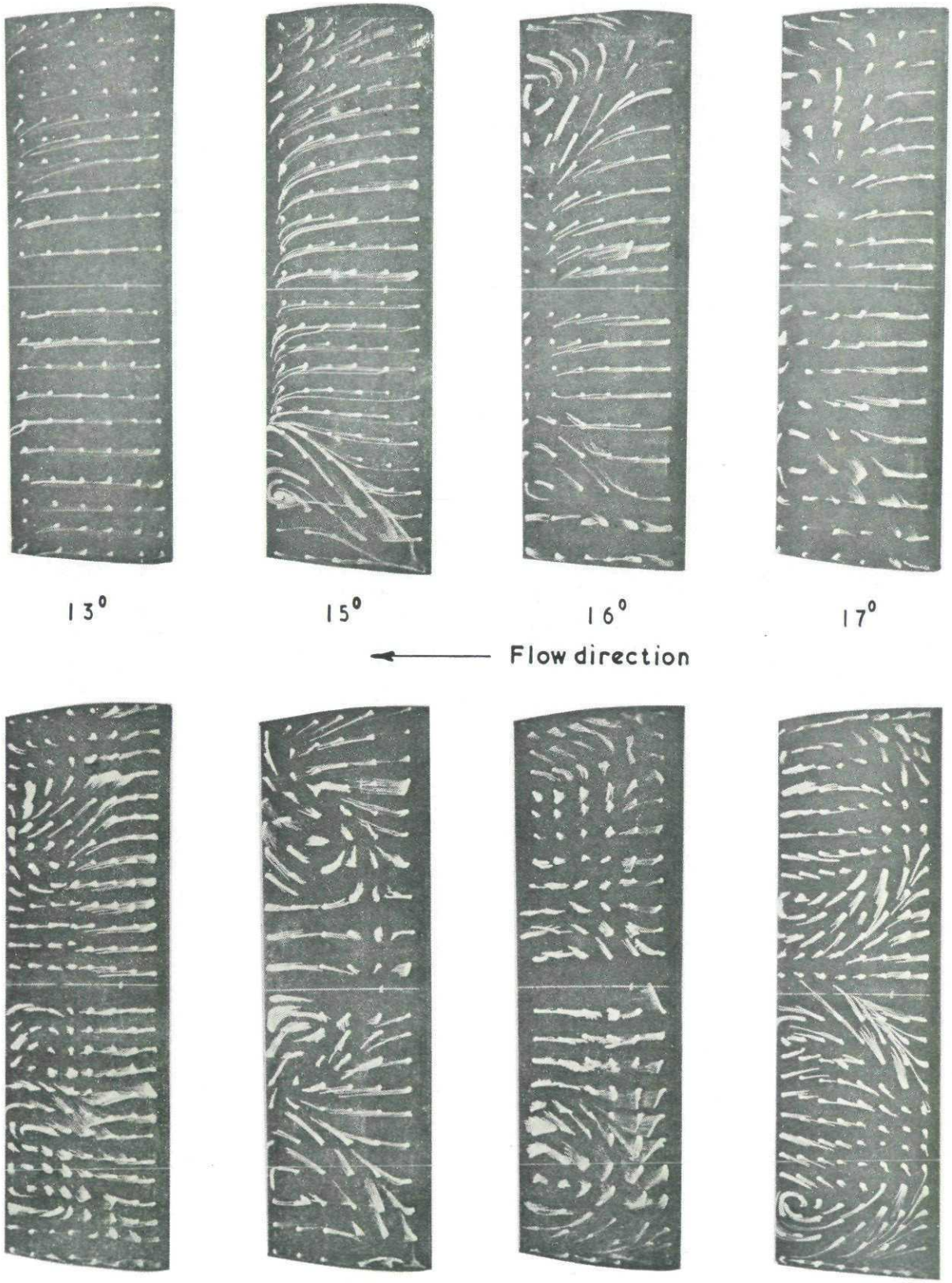

Oil-flow patterns at M=0·16 on NPL 9619 section. Span/chord = 3·29.
$R_c = 3{\cdot}14 \times 10^6$. No boundary-layer control.

FIG. 8

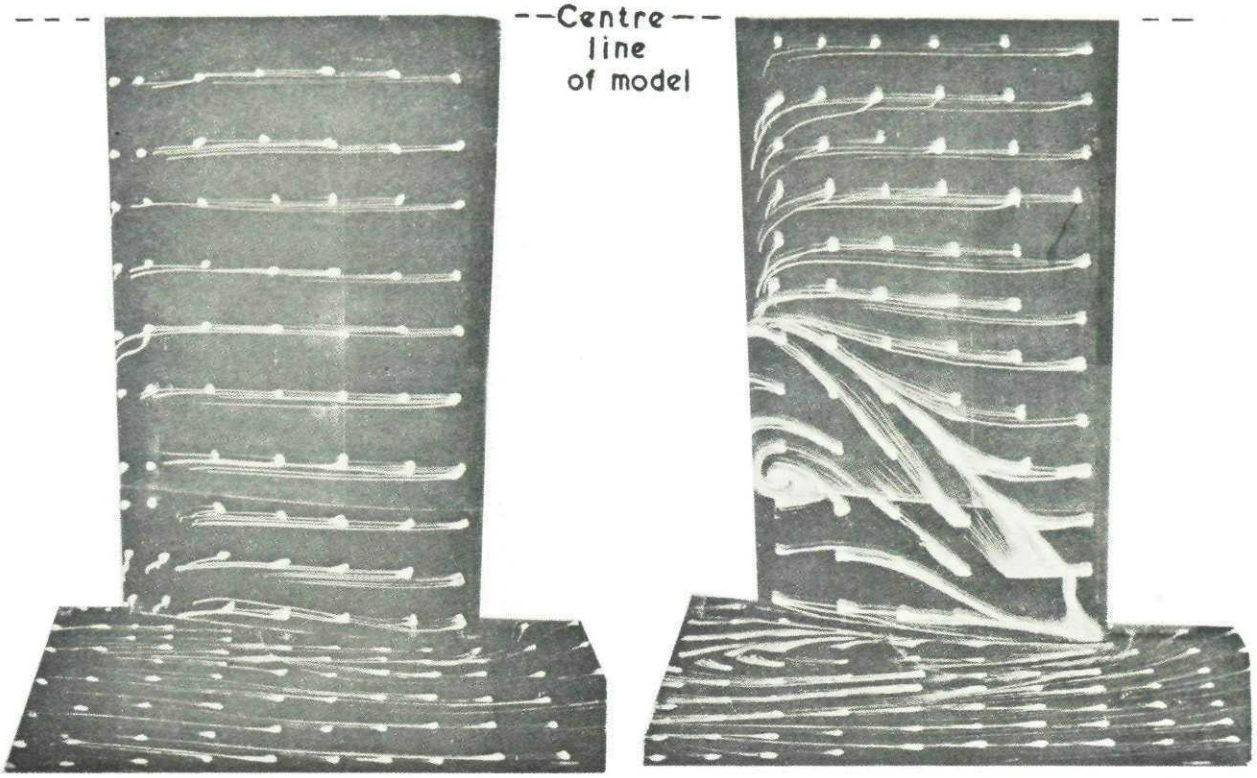

(a) Flow with attached flow in corner, at 13°, and as at 19°, 20°

(b) Flow with corner separation at 15° and as at 16°–18°

Flow direction ←

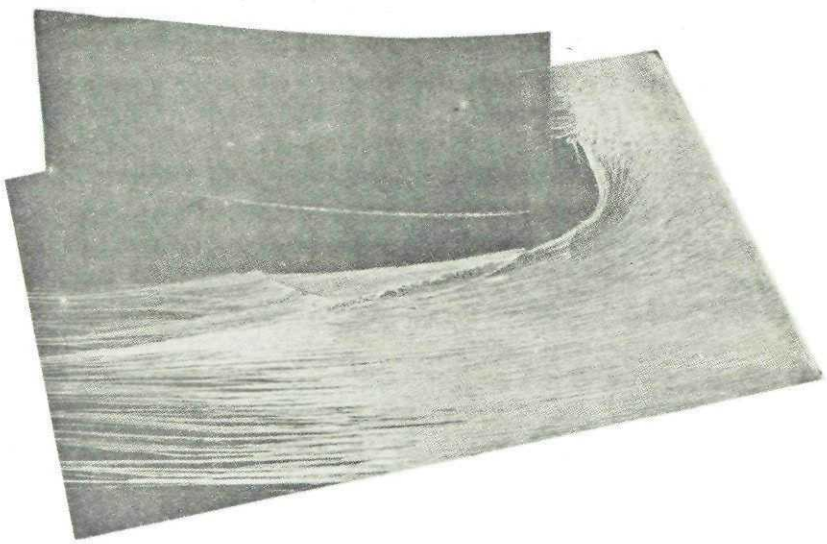

(c) Oil-flow pattern showing position of three-dimensional separation line at 20°

Examination of end-wall flow patterns. $R_c = 3{\cdot}14 \times 10^6$

No boundary-layer control.

FIGS. 9, 12, 13

FIG. 13 Oil-flow pattern at 18° on centre portion of NACA 0012 aerofoil. Span/chord = 1·4 between fins. $R_c = 2{\cdot}88 \times 10^6$

FIG. 9 Alternate régime at 20° with upper slots and perforations unsealed. NPL 9619 aerofoil. Span / chord = 3·29. $R_c = 3{\cdot}14 \times 10^6$. No boundary-layer control.

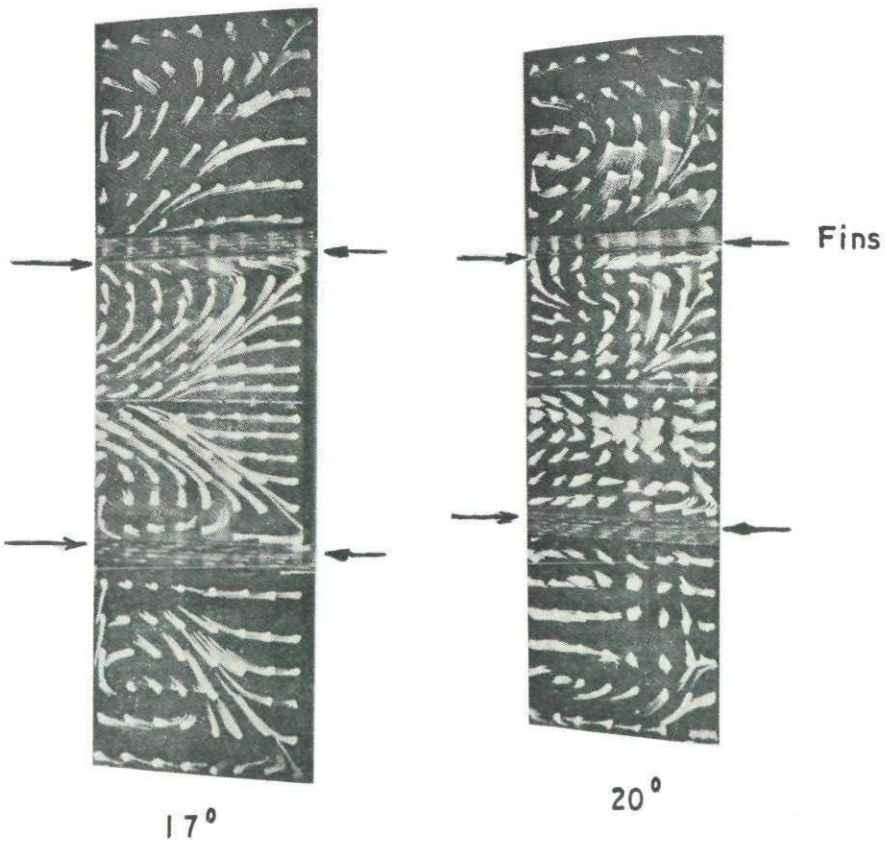

FIG. 12 Oil-flow patterns on NPL 9619 with span/chord = 1·28 between fins and thickened boundary layers on inside surfaces of fins. $R_c = 3{\cdot}14 \times 10^6$.

FIG.10

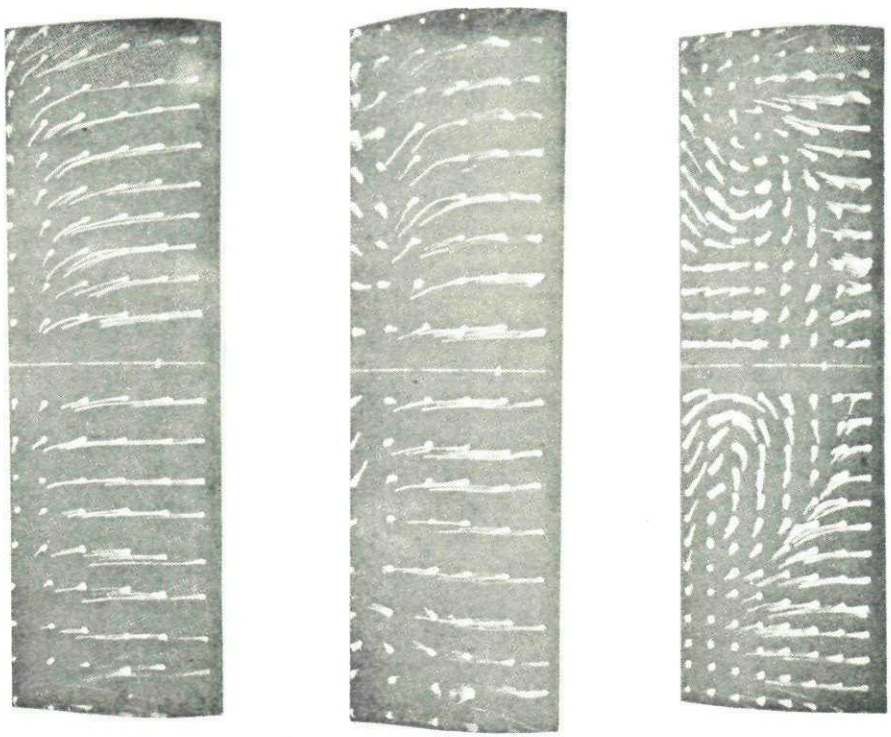

15° 17° 17·5°

Flow direction

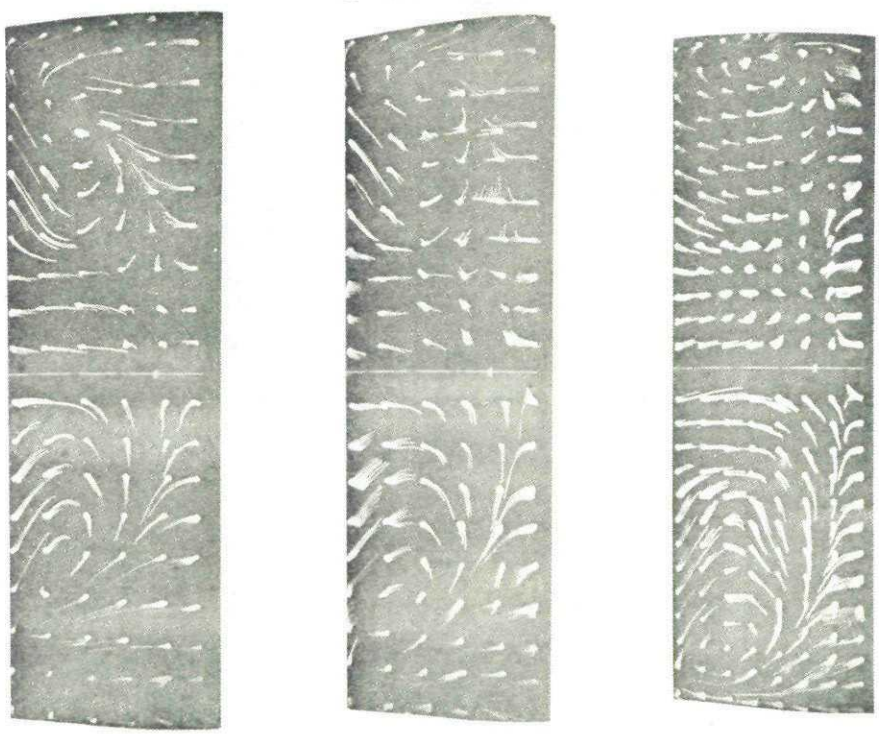

18° 19° 20°

Geometric incidence

Oil-flow patterns at M=0·16 on NPL 9619 section. Span / chord = 3·29. R_c = 3·14 x 10^6. Boundary-layer removal at floor slots and suction into 0·18 c length of perforations at each end of span, C_Q = 0·0018.

FIG. 11

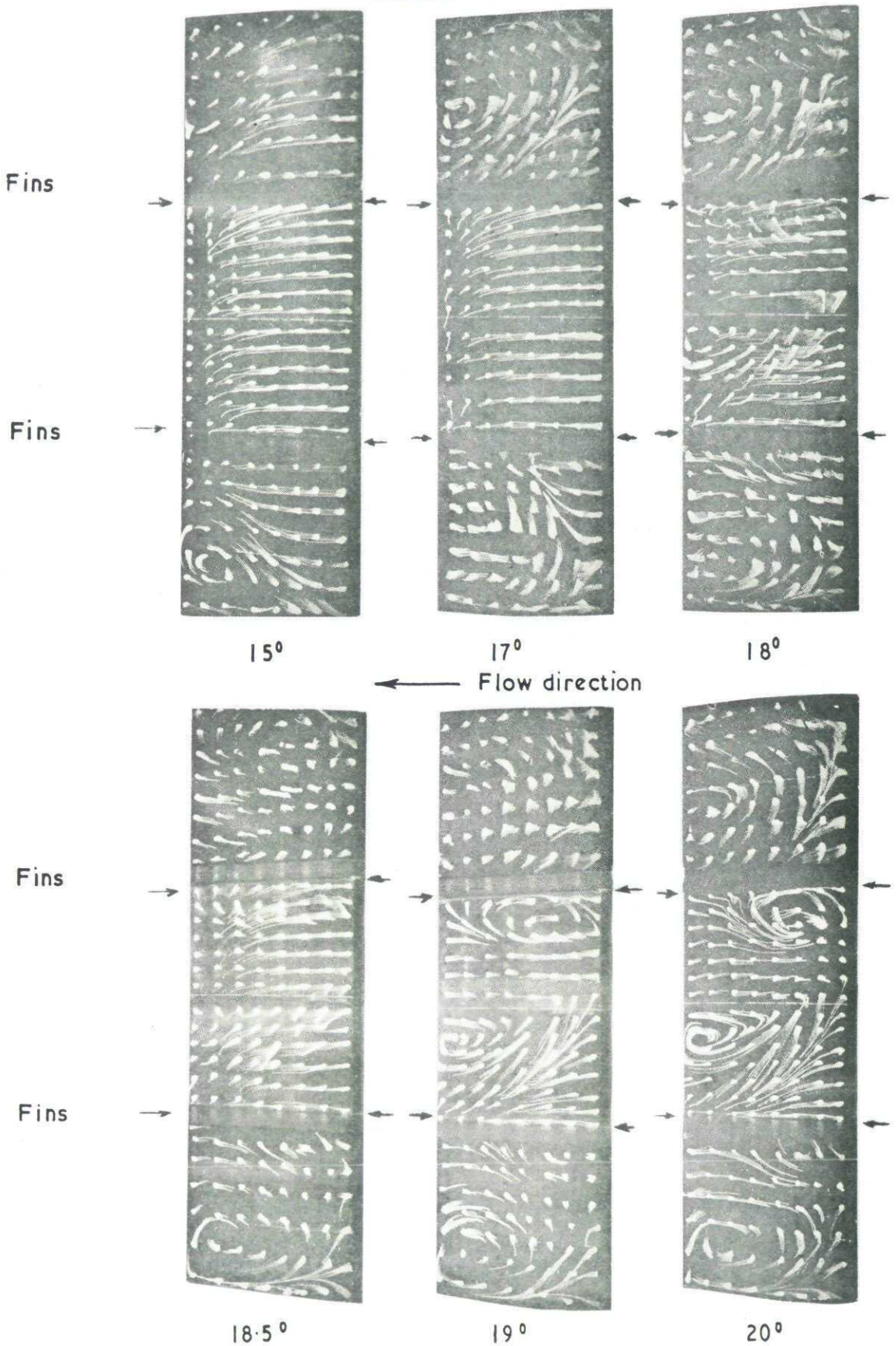

Oil-flow patterns at M = 0·16 on NPL 9619 section with span/chord = 1·28 between fins. $R_c = 3 \cdot 14 \times 10^6$. No boundary-layer control

FIG.14

Oil-flow patterns at M=0·16 on NACA 0012 section.

Span/chord = 6·0 . $R_c = 0{\cdot}76 \times 10^6$.

FIG.15

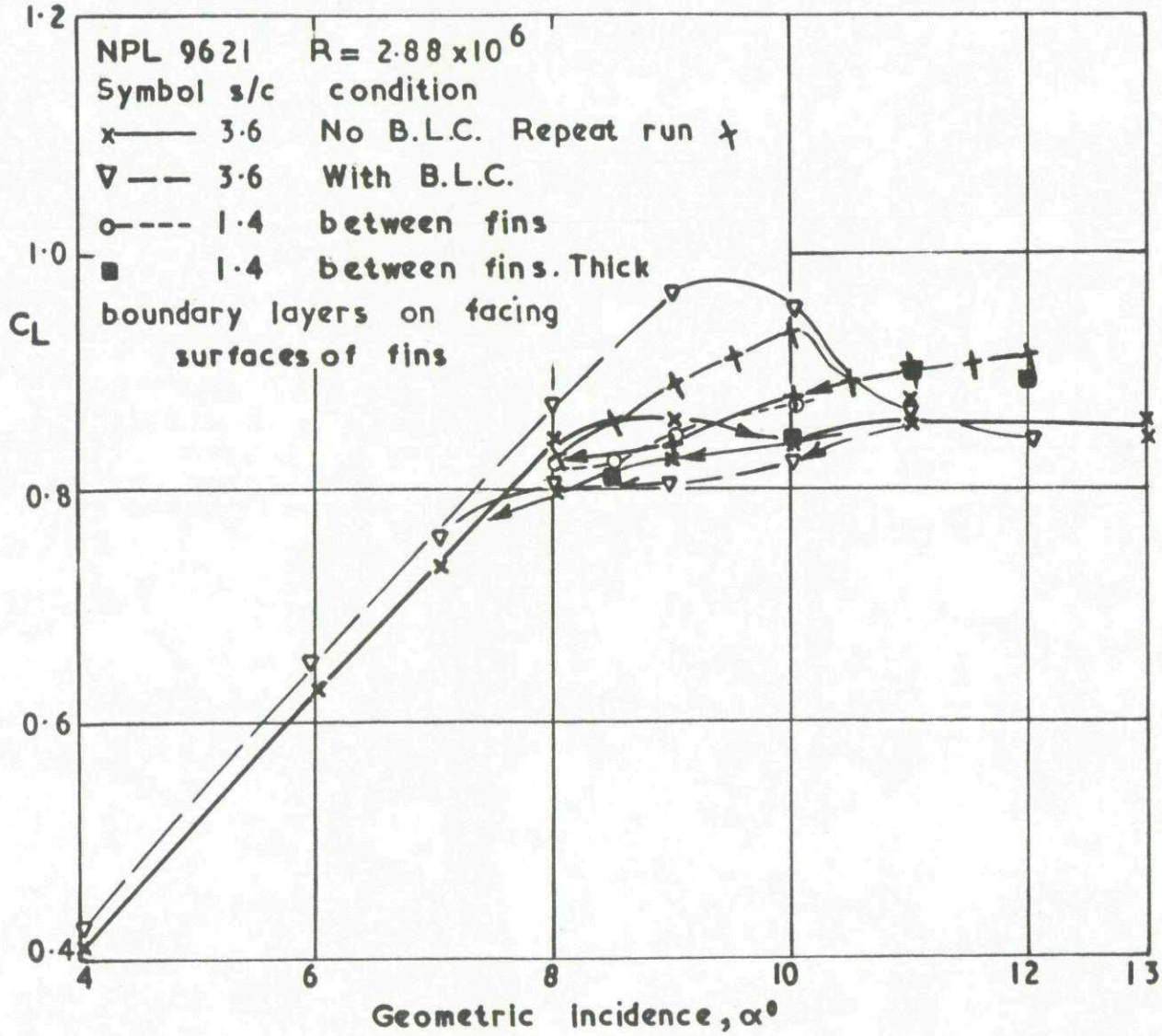

Variation of lift coefficient with incidence for NPL 9621 in various conditions, showing hysteresis loops

FIG.16

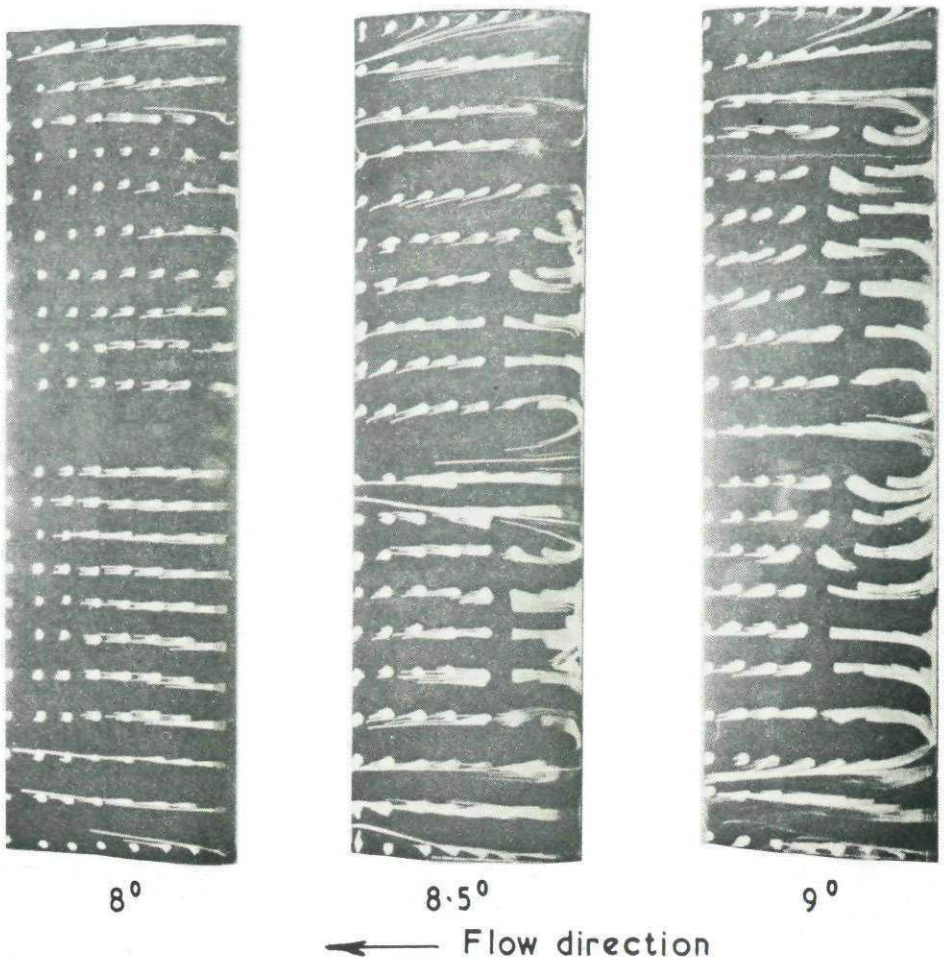

Oil-flow patterns at M=0·16 on NPL 9621 section with span / chord = 3·6 . $R_c = 2{\cdot}88 \times 10^6$. No boundary-layer control .

FIG.17

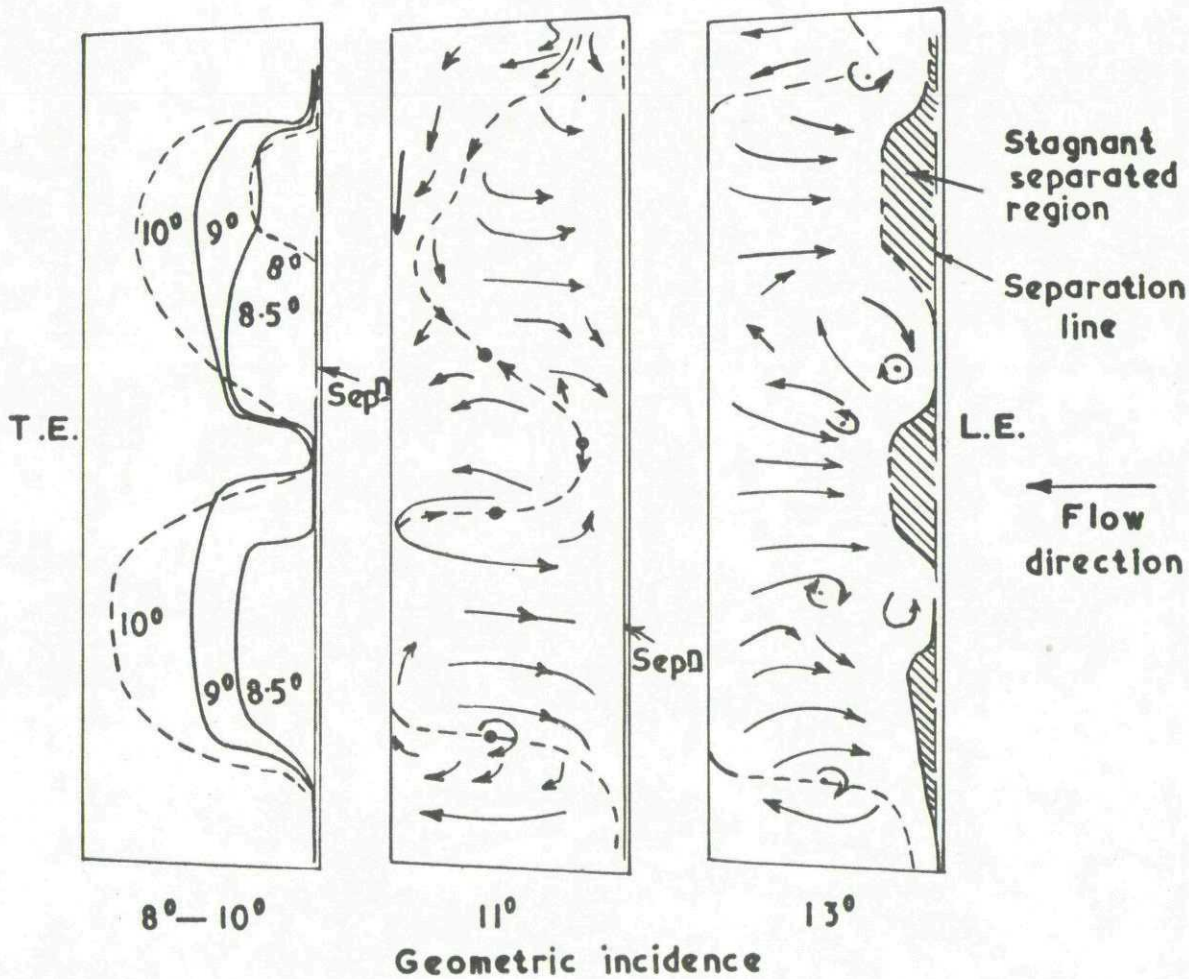

Variation with incidence of the re-attachment lines observed in Fig.16

FIGS. 18 & 19

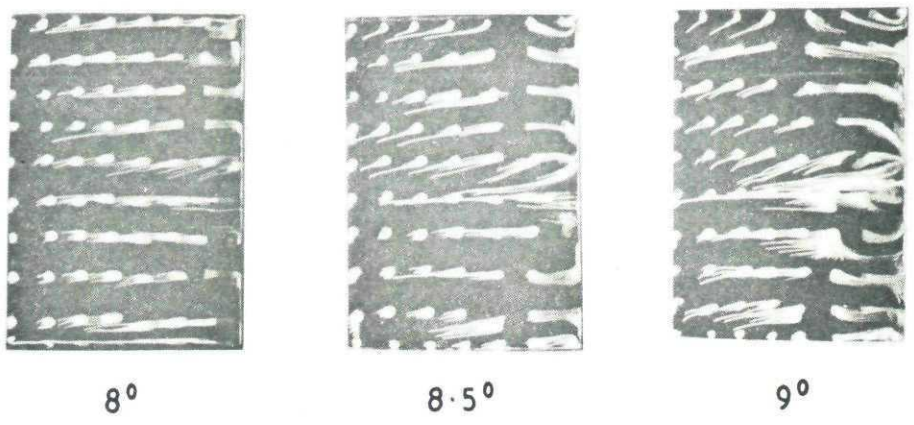

8° 8·5° 9°

Flow direction

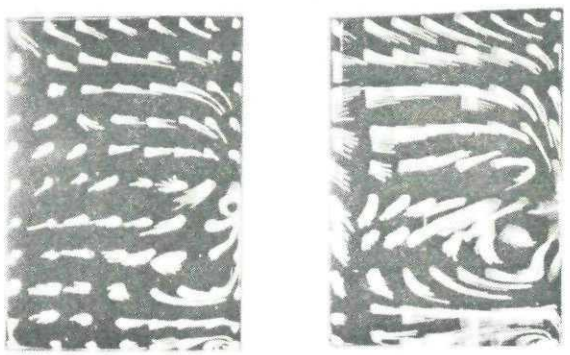

10° 11°

Geometric incidence

FIG. 18 Oil-flow patterns on NPL 9621 section with span / chord = 1·4 between fins. $R_c = 2{\cdot}88 \times 10^6$

8·5° 10° 12°

Geometric incidence

FIG. 19 Oil-flow patterns on NPL 9621 section with span / chord = 1·4 between fins and thickened boundary layers on inside surfaces of fins.

A.R.C. C.P. No.1146
January, 1970
Gregory, N., Quincey, V. G., O'Reilly, C. L. and Hall, D. J.

PROGRESS REPORT ON OBSERVATIONS OF THREE-DIMENSIONAL FLOW PATTERNS OBTAINED DURING STALL DEVELOPMENT ON AEROFOILS, AND ON THE PROBLEM OF MEASURING TWO-DIMENSIONAL CHARACTERISTICS

Three-dimensional patterns were obtained in appreciable regions of separated flow on both thick and thin aerofoils at high and low Mach numbers. A form of boundary-layer control prevented separation of flow in the corners at the aerofoil ends but did not inhibit development of the three-dimensionality.

Further/

A.R.C. C.P. No.1146
January, 1970
Gregory, N., Quincey, V. G., O'Reilly, C. L. and Hall, D. J.

PROGRESS REPORT ON OBSERVATIONS OF THREE-DIMENSIONAL FLOW PATTERNS OBTAINED DURING STALL DEVELOPMENT ON AEROFOILS, AND ON THE PROBLEM OF MEASURING TWO-DIMENSIONAL CHARACTERISTICS

Three-dimensional patterns were obtained in appreciable regions of separated flow on both thick and thin aerofoils at high and low Mach numbers. A form of boundary-layer control prevented separation of flow in the corners at the aerofoil ends but did not inhibit development of the three-dimensionality.

Further/

A.R.C. C.P. No.1146
January, 1970
Gregory, N., Quincey, V. G., O'Reilly, C. L. and Hall, D. J.

PROGRESS REPORT ON OBSERVATIONS OF THREE-DIMENSIONAL FLOW PATTERNS OBTAINED DURING STALL DEVELOPMENT ON AEROFOILS, AND ON THE PROBLEM OF MEASURING TWO-DIMENSIONAL CHARACTERISTICS

Three-dimensional patterns were obtained in appreciable regions of separated flow on both thick and thin aerofoils at high and low Mach numbers. A form of boundary-layer control prevented separation of flow in the corners at the aerofoil ends but did not inhibit development of the three-dimensionality.

Further/

A.R.C. C.P. No.1146
January, 1970
Gregory, N., Quincey, V. G., O'Reilly, C. L. and Hall, D. J.

PROGRESS REPORT ON OBSERVATIONS OF THREE-DIMENSIONAL FLOW PATTERNS OBTAINED DURING STALL DEVELOPMENT ON AEROFOILS, AND ON THE PROBLEM OF MEASURING TWO-DIMENSIONAL CHARACTERISTICS

Three-dimensional patterns were obtained in appreciable regions of separated flow on both thick and thin aerofoils at high and low Mach numbers. A form of boundary-layer control prevented separation of flow in the corners at the aerofoil ends but did not inhibit development of the three-dimensionality.

Further/

Further experiments are planned to measure the spanwise load distribution associated with the three-dimensionality, which it is hoped can be suppressed by the use of distributed suction on the end walls.

Further experiments are planned to measure the spanwise load distribution associated with the three-dimensionality, which it is hoped can be suppressed by the use of distributed suction on the end walls.

Further experiments are planned to measure the spanwise load distribution associated with the three-dimensionality, which it is hoped can be suppressed by the use of distributed suction on the end walls.

Further experiments are planned to measure the spanwise load distribution associated with the three-dimensionality, which it is hoped can be suppressed by the use of distributed suction on the end walls.

Produced and published by
HER MAJESTY'S STATIONERY OFFICE

To be purchased from
49 High Holborn, London WC1V 6HB
13a Castle Street, Edinburgh EH2 3AR
109 St Mary Street, Cardiff CF1 1JW
Brazennose Street, Manchester M60 8AS
50 Fairfax Street, Bristol BS1 3DE
258 Broad Street, Birmingham B1 2HE
80 Chichester Street, Belfast BT1 4JY
or through booksellers

Printed in England

C.P. No. 1146

SBN 11 470394 9